The Journal of Experimental Biology 212, 2731-2745
Published by The Company of Biologists 2009
doi:10.1242/jeb.026922

Kinematics, hydrodynamics and force production of pleopods suggest jet-assisted walking in the American lobster (*Homarus americanus*)

Jeanette L. Lim* and M. Edwin DeMont

Department of Biology, St Francis Xavier University, PO Box 5000, Antigonish, NS, Canada, B2G 2W5

*Author for correspondence (jlim@oeb.harvard.edu)

Accepted 2 June 2009

SUMMARY

The American lobster (*Homarus americanus*) displays a diverse set of locomotory behaviours that includes tail flips, walking and paddling. Paddling is carried out by the four pairs of paddle-shaped pleopods on the ventral abdomen. Although it is recognized that pleopod-generated fluid flows have some locomotory role in adults, reports on their relative importance in locomotion are inconsistent. This paper integrates experimental kinematics and hydrodynamics of lobster pleopod beating to determine the mechanism and magnitude of pleopod force production. A kinematic analysis of pleopod beating in live lobsters showed that the pleopods execute an adlocomotory metachronal beating pattern. We modelled *in vivo* pleopod kinematics with a set of simple trigonometric functions, and used these functions to program a mechanical lobster model consisting of motor-driven pleopods on a lobster abdomen exoskeleton. Based on flow visualizations obtained from applying particle image velocimetry to the lobster model, we propose that the unsteady metachronal kinematics of the pleopods can maximize thrust by exploiting forces arising from individual pleopod activity and interactions among adjacent pairs. The pleopods continuously entrain fluid surrounding the lobster and create a caudally directed fluid jet oriented parallel to the substratum. Inputting wake morphology and velocity data into a simplified model for steady jet thrust showed that the pleopods of the lobster model produced 27–54 mN of thrust, which is comparable to the propulsive forces generated by other proficient swimmers. These results suggest that lobster pleopods are capable of producing forces of a magnitude that could assist the walking legs in forward propulsion.

Key words: lobster, *Homarus americanus*, pleopod, locomotion, hydrodynamics, metachrony, kinematics, robotics, jet wake.

INTRODUCTION

Using tail-flips, walking and paddling to navigate its ocean bottom habitat, the American lobster (*Homarus americanus* Milne-Edwards) exemplifies diversity in aquatic locomotory mechanisms (Herrick, 1909). In lobsters and several other crustaceans, paddling is carried out by a series of paired appendages on the ventral abdomen, the swimmerets or pleopods. Although the mechanics of tail-flips and walking have been fairly well explored in crustaceans (e.g. Cattaert and Clarac, 1983; Mitchell and DeMont, 2004; Nauen and Shadwick, 1999; Nauen and Shadwick, 2001) the question of pleopod function in lobster locomotion has received little quantitative treatment. *H. americanus* is important commercially on the east coast of Canada and the United States (Campbell, 1989; Cooper and Uzmann, 1971), and physical limitations on movement in the environment will influence the distribution of these animals in space and time. Knowledge about the lobster's locomotory abilities may be applied in the management of this fishery that operates on discrete fishing regions (Campbell, 1989; Comeau and Savoie, 2002).

The American lobster has four pairs of biramous paddle-shaped pleopods, each consisting of a stalk (protopod) and two distally attached and approximately elliptical rami (exopod, endopod) that bear a fringe of setae (Herrick, 1909). The movement of pleopod pairs is coordinated in an adlocomotory metachronal sequence: the most posterior pair initiates its power and recovery stroke cycle followed in succession by the remaining pairs, such that the metachronal wave travels in the same direction as the body (Davis, 1969; Sleigh and Barlow, 1980). Rhythmic beating of the pleopods under the raised abdomen creates flows around the lobster that have a role in chemical signalling, egg ventilation and equilibrium responses (Atema and Voigt, 1995; Davis, 1968a; Govind et al., 1995). In the benthic adult stage, the pleopods purportedly assume a secondary role in locomotion by assisting the thoracic walking legs especially during high-speed walking or while climbing obstacles (Atema and Voigt, 1995; Cattaert and Clarac, 1983; Davis, 1968b).

Previous work on the paddling pleopods in lobsters and other crustaceans has focused on the neuromuscular control and kinematics of the appendages (Copp and Hodes, 2001; Davis, 1968a; Davis, 1968b; Davis, 1968c; Stamhuis and Videler, 1998a). Davis's (Davis, 1968c) seminal analysis of pleopod beating in *H. americanus* provides data on several kinematic variables, including beat frequency, periods of the power and recovery strokes, and phase shifts between adjacent pleopod pairs. Despite the importance of these quantities in characterizing pleopod activity, they only implicitly define the dynamics of the coordinated multi-paddle system.

Also, references to pleopod fluid mechanics and their force-generating capabilities in *H. americanus* have been largely qualitative. The pleopods are generally described as oscillating paddles that draw fluid toward the body and create currents (Atema, 1985), producing thrust through a drag-based mechanism (Lochhead, 1977; Wootton, 1999). Several studies using flow visualization techniques to quantify the hydrodynamics of multi-limbed systems in small, pelagic or tube-dwelling crustaceans have revealed that the wake behind the set of paddling appendages is a caudally directed jet (Stamhuis and Videler, 1998b; van Duren and Videler, 2003; Yen et al., 2003); however, the flow regime experienced by bottom-dwelling lobsters, the largest of the swimming crustaceans

(Lochhead, 1977), may impose different mechanical constraints on their pleopods. In a study on the role of pleopods in equilibrium responses in *H. americanus*, Davis (Davis, 1968a) visualized flows around the pleopods by filming the motion of suspended particles in the fluid. Through this qualitative analysis, he concluded that pleopod-generated flows have a predominant rearward direction, but he also remarked on the difficulty in quantifying pleopod forces because of the turbulent flow regime and changes in pleopod morphology throughout the beat cycle. Adding to the complexity are the numerous opportunities for interactions between flows produced by each pleopod pair in the coordinated multi-paddle system (Stamhuis and Videler, 1998c), as well as their interaction with the nearby ground. Davis (Davis, 1968a) determined 'hypothetical forces' with arbitrary units for comparison between high and low frequency pleopod beating, but was unable to provide absolute quantities.

Associated with this lack of quantified pleopod forces is debate over whether the pleopods are even capable of generating forces that are large enough to have a significant role in locomotion (Atema and Voigt, 1995; Ayers, 2004; Cattaert and Clarac, 1983; Davis, 1968a; Govind et al., 1995). Davis (Davis, 1968a) proclaimed the importance of pleopod-generated forces when he demonstrated that pleopods in *H. americanus* perform a crucial role in producing righting torques, which are produced when lobsters are tilted off axis. Conversely, Cattaert and Clarac (Cattaert and Clarac, 1983) suggested that the small forces generated by pleopods in the morphologically similar *H. gammarus* were unlikely to make a substantial contribution to forward propulsion.

In this paper, we determine the time-varying position of lobster pleopods and use these data to program the motion patterns of a physical lobster model. We apply the quantitative flow visualization technique of particle image velocimetry to the mechanical model to characterize the flow field near the pleopods, and integrate pleopod kinematics and hydrodynamics to propose a mechanism of pleopod force production in the American lobster. We begin to answer the question of whether pleopods can play a significant role in lobster locomotion by quantifying pleopod thrust from the mechanical model. We compare the force estimates to the thrust produced by other aquatic animals, and show that the pleopods could contribute to a jet-assisted walking mechanism in the American lobster.

MATERIALS AND METHODS

Experimental animals

Live adult lobsters (*Homarus americanus*) were obtained directly from a fishing boat at Bayfield, Nova Scotia, Canada. Animals were transported to the St Francis Xavier University Animal Care facility in Antigonish, NS, and transferred to circulating seawater (8–10°C, 35‰) tanks where they were maintained in the dark and fed a bi-weekly diet of fish (various species). All procedures and experiments adhered to guidelines of the St FXU Animal Care Committee.

Kinematics of pleopod beating in live lobster

Film records of pleopod beating were obtained from individual lobsters in a 100 l aquarium of seawater maintained at 9–11°C. Lobsters were placed on a Lexan sheet ramp positioned at a 20 deg. incline in the aquarium, and were induced to walk with pleopods beating using an aversive light stimulus placed at the bottom of the ramp. A high-speed video camera (512×480 pixels, Photron Fastcam PCI R2, Photron, San Diego, CA, USA) filmed the lateral aspect (left side) of the lobster (250 frames s^{-1}, 2 ms shutter speed). It was assumed that the left and right pleopods in a pair beat synchronously (Davis, 1968c). Sequences of walking accompanied by pleopod beating were recorded for three lobsters ranging from 309 to 1019 g in body mass (161 to 226 mm in body length, approximated as carapace length plus abdomen length). Two different walking sequences from a female lobster (308.6 g body mass, 161.3 mm body length) were suitable for further detailed analysis of pleopod motion patterns, and data from one of these walking sequences are presented here as a representative sequence.

Following filming, the lobster was weighed, killed, and then morphometric measurements were taken. Body dimensions were measured with Vernier calipers and were defined as in MacCormack and DeMont (MacCormack and DeMont, 2003). Pleopod morphometrics were measured from digital photographs using ImageJ software (v1.33u, NIH, Bethesda, MD, USA). The linear dimensions of the pleopods were taken as the largest distances across the structure being measured. Approximating total pleopod length as endopod length plus protopod length, pleopod length averaged over the four paddle-shaped pairs was 30±2 mm (± s.d.). Complete morphological data for the lobster used in the kinematic analysis are presented in Lim (Lim, 2006).

The mean pleopod beat frequency was measured directly from the video images as the inverse of the period of one beat cycle (power and recovery stroke). Photron Motion Tools software (v.1.0.6.1) was used to manually digitize points in each image frame. For each pleopod pair (anterior-most pair is PP1, posterior-most is PP4), position data were recorded for (1) the pleopod tip, (2) the centre of the internal pleopod joint (between the protopod and rami), (3) the point of articulation between the sixth abdominal segment and the telson (centre of the tail fan), and (4) a point on the lateral side of the lobster where the fifth and sixth abdominal segments meet (Fig. 1A). Points 3 and 4 were used to define the long body axis. Pleopod movement was best resolved by analyzing every third video frame (83 frames s^{-1}), which still satisfied the requirements of Nyquist sampling and could resolve the full range of pleopod motion (Press et al., 1989).

Models for pleopod motion

The pleopod and body position data were used to determine the time-varying angle of the pleopod with respect to the body's long axis, denoted by β. Because the location of the point where the pleopod pivots with the ventral abdomen was obstructed by the overhanging pleura of the exoskeleton in the video images, it was necessary to develop a model to estimate the angle from the available position data. Assuming that a pleopod is fully extended during its power stroke, the straight line running through the pleopod tip and joint will also run through the protopod. The angle at the intersection of this line (the pleopod long axis) with the straight line defining the long body axis approximates the pleopod angle β during the power stroke (Fig. 1B). For the recovery stroke, however, this method gives incorrect angles because the pleopod joint bends and the rami are no longer in line with the protopod. Nevertheless, the measured power stroke angles can be used to estimate the location of the pleopod-abdomen pivot. The angle of the protopod relative to the horizontal (θ) can be calculated from β, and the length of the protopod is known; trigonometry gives the coordinates of the pivot position from these data. Observation of the video records showed that the lobster kept its abdomen relatively straight during walking. Assuming that the abdomen does not flex or extend, the spatial relationship between the pivot and the two recorded reference points on the body is fixed. This relationship can be defined by the length of the line connecting the pivot and the telson, and the angle between

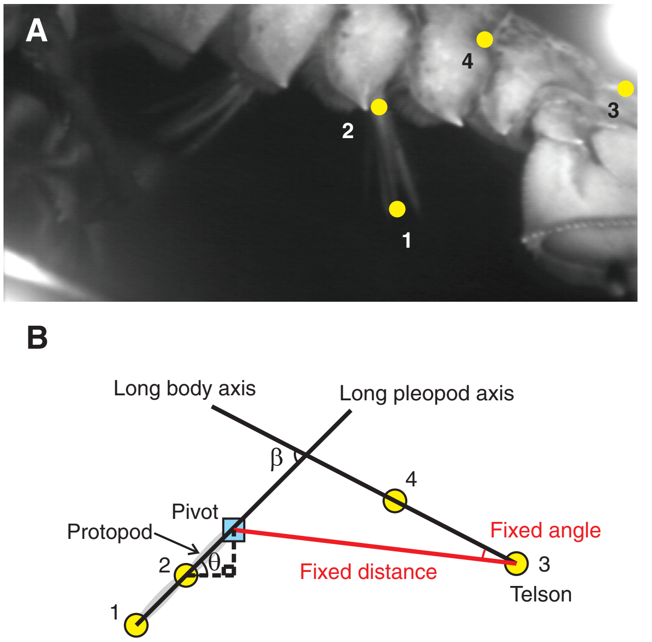

Fig. 1. (A) Locations of digitized points on the lobster's body and pleopods for the kinematic analysis of pleopod beating. (1) Pleopod tip, (2) centre of the pleopod joint, (3) articulation between the sixth abdominal segment and the telson, and (4) articulation between fifth and sixth abdominal segments. (B) Schematic diagram of the model used to determine the angle β between the pleopod (shown in grey) and the long body axis. Pleopod and body position data (yellow circles) were used to calculate θ (the angle between the protopod and the horizontal), and define a fixed spatial relationship among the body reference points and the estimated location of the pleopod pivot (blue square).

this line and the long body axis. With the fixed relationship defined, the pivot position can then be estimated for the rest of the beat cycle using the available data on the body reference points. The pleopod angle β is then measured for the entire beating bout of each pleopod pair.

Following Stamhuis and Videler (Stamhuis and Videler, 1998a), the pleopod angle data were transformed with the fast Fourier transform (FFT) function in MatLab (v.7, R14, MathWorks, Natick, MA, USA) to identify the major frequency components of the pleopod motion. In cases where position data were unavailable for a portion of a pleopod beat cycle because of obstruction by the walking legs, an interpolating polynomial was used to interpolate angle data and produce a data set of evenly spaced points. We chose to use polynomial interpolation to avoid biasing our data toward a periodic pattern. The power of the harmonics present in the signal was computed as the squared magnitude of the transformed data and plotted against frequency to yield a power spectrum (Press et al., 1989). Transformed pleopod angle data were used to derive simplified trigonometric functions that approximate pleopod motion in the time domain.

Mechanical lobster model

A mechanical lobster model was built from the exoskeleton of an adult American lobster obtained live from a local supplier in Antigonish, NS. The use of a physical model instead of a live lobster ensures that the pleopod beating behaviour can be performed repeatedly, consistently, and on cue (Alexander, 2003; Koehl, 2003).

Immediately following death of a lobster, the abdomen was severed from the cephalothorax and a 10 mm-wide strip of exoskeleton running the length of the abdomen was cut from the dorsal surface to facilitate removal of the internal soft tissue with forceps, leaving an eviscerated and intact exoskeleton. The exoskeleton's hardness was inspected by hand to ensure recently molted lobsters were not used, and experiments were performed immediately after dissection to ensure retention of the exoskeleton's natural mechanical properties. Building a physical model from the isolated exoskeleton of a real lobster afforded full mechanical control over the movement of the system, while allowing critical morphological features and material properties to be retained. Two different male lobsters were used for the mechanical model. The pleopod hydrodynamics for one of the lobsters in the model [1240 g full body wet mass, 235.8 mm body length, 41±5 mm (mean ± s.d.) pleopod length; complete morphological data in Lim (Lim, 2006)] were subsequently analyzed in detail.

Small holes drilled into the exoskeletal walls of the four abdominal segments with paddling pleopods gave internal access to the joint between the pleopods and the abdomen. Each pleopod was coupled to a mini servomotor (Parallax, Rocklin, CA, USA) *via* an L-shaped wire rod (Fig. 2A); the short arm of the rod was inserted into the protopod, while the long arm passed through the drilled hole opposite the pleopod and connected to a motor held above the exoskeleton in a metal bracket (Fig. 2B). The distal rami of the pleopods could not be actively controlled given this coupling arrangement in our model, so their resulting motion was entirely passive. The motors enabled planar pleopod motion, which was controlled with computer software (Parallax Servo Controller Interface v0.9h Beta, Parallax) that communicated with the motors *via* a Parallax Servo Controller USB interface card. Six volts from an external DC power supply was used to run the motors. The two motors associated with a pleopod pair were wired such that their rotation mirrored each other and pleopods on the same segment beat in synchrony. The trigonometric functions derived for each pleopod

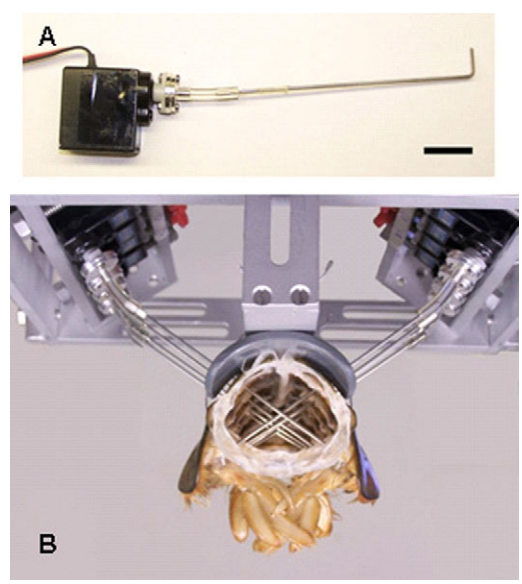

Fig. 2. (A) Servomotor used to drive pleopod beating in a mechanical lobster model. An L-shaped wire rod and short segment of polyvinyl tubing were used to couple the motor to a pleopod. Scale bar, 20 mm. (B) Anterior view of the assembled mechanical lobster model. Metal brackets held the servomotors and exoskeleton together.

pair (see Results) were used to define animation sequences that were run with the servo controller software.

The lobster model was held in a fixed position in a 100 l aquarium of fresh water (20°C) by metal rods that were attached to the rim of the aquarium. Fixing the position of the model is a simplification that is still biologically relevant, as there can be instances when a lobster is attempting to ascend an obstacle but is not making any forward progress. A Lexan sheet positioned approximately 60 mm below the ventral surface of the model simulated a horizontal ground surface. Experimental variables were set such that the flow conditions would be similar to those for a lobster paddling in the ocean. The model was sufficiently far from the wall and operated at a large enough Reynolds number (*Re*) to avoid wall effects. The distance between the model and water surface (~2 pleopod lengths) was constrained by the need to keep the servomotors above water, but no significant surface effects (e.g. surface ripples) were observed while the model was operating. The lobster model executed approximately eight complete pleopod beat cycles over a period of 6–7 s, resulting in a beat frequency of ~1.3 Hz that functioned as a representative value for the size of lobster used in the model.

Quantifying the pleopod flow field

A commercial particle image velocimetry (PIV) system (Dantec Dynamics, Ramsey, NJ, USA) was used to quantify flows in planar sections of the flow field surrounding the pleopods. A Nd:YAG double-cavity pulsed laser (New Wave Research, Fremont, CA, USA) directed through a lens created a 1–2 mm-thick light sheet that illuminated a two-dimensional slice of water in the aquarium seeded with 20 μm-diameter polyamide beads. The light sheet was projected in multiple planes parallel to the model's long body axis (Fig. 3) and imaged with a video camera (30 frames s^{-1}, 1008×1016 pixels; Kodak Megaplus ES 1.0, Eastman Kodak, San Diego, CA, USA) in separate trials. Flows in the lobster model's sagittal (*xy*) and two parasagittal planes (20 and 30 mm left of sagittal) were visualized by reflecting the laser off a mirror angled at 45 deg. beneath the glass bottom of the aquarium, while flows in a frontal (*xz*) plane just intersecting the fully extended pleopods were visualized by firing the laser directly behind the lobster model. Flows were assumed to be bilaterally symmetrical, given the synchronous beating of the left and right pleopods in a pair. The model was manually triggered to begin its animation sequence at the start of laser firing.

Dantec Dynamics's FlowManager v4.50 software was used for all data acquisition and analysis. Video recordings were calibrated from images of a Plexiglas block with known dimensions. A two-dimensional FFT-based cross-correlation routine performed on the particle images produced a 43×44 matrix of velocity vectors (64×64 pixel interrogation area, 65% overlap, Gaussian fit peakfinder). These analysis parameters and the laser pulse interval used minimized the effect of data quality loss due to unpaired particles, given the seeding density and speed of the pleopod flows. The raw vector map was validated by removing zero-velocity vectors and manually deleting obvious erroneous vectors (vectors that drastically differed from their neighbours in magnitude and direction, often found near the edges of the imaged flow field). An automated spline interpolation routine filled the resulting gaps in the vector map. To remove noise that would otherwise be amplified in subsequent calculations with the velocity vectors, final vector maps were produced by applying an average filter to the validated maps. Each original vector was replaced with a vector representing the uniformly weighted average of neighbouring vectors in a 3×3 window. Images of the velocity vector fields presented in this paper display every second vector for clarity; however, the entire matrix was used for subsequent calculations that used flow velocity data. Quantities such as mean vector angles and magnitude in specific regions of the flow field were computed using a custom MatLab program (written by Eric Tytell, Harvard University, 2005) that allows the user to manually select and analyze specific regions of interest in the velocity vector field.

Information from two-dimensional flow fields measured in orthogonal planes can be combined to estimate the three-dimensional flow morphology (e.g. Drucker and Lauder, 1999; Drucker and Lauder, 2000). Because data are collected in separate trials, this analysis assumes low variability in the propulsor's motion patterns between independent trials (Drucker and Lauder, 1999). The mechanical model was well suited for this application as it could perform the same kinematic sequence repeatedly. For the model's eight-cycle beating bout, 30–90 image pairs were recorded in each image plane, depending on the specific laser plane orientation. Velocity vector and vorticity fields were computed for a total of 450 image pairs.

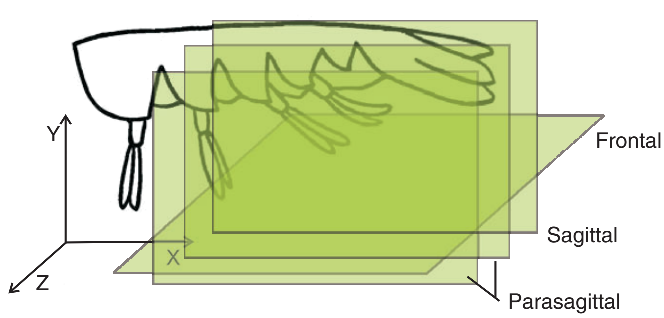

Fig. 3. Orientation of the light sheet planes (sagittal, 2 parasagittal, and frontal) in which pleopod flows were visualized. Only the four left pleopods are shown. The axes indicate the coordinate system that was used.

RESULTS

Pleopod kinematics in live lobster

The oscillating pleopods execute an adlocomotory metachronal sequence with PP4 leading the cycle (Fig. 4). For the pleopod beating sequence presented here, the mean (±s.d.) half-cycle angle swept is 1.83±0.29 rad. There is a clear metachronal pattern among the power strokes, whereas the pleopods are more physically grouped together for a portion of their recovery strokes as a result of differences in maximum angles obtained by each pair. Each pleopod pair performs its periodic motion pattern without obstruction from its neighbouring pairs during the majority of the power stroke phase. Manually overlapping the four pleopod angle curves gave a visual indication that the different pleopod pairs appear to have similar angular velocities, which are relatively constant during the power and recovery strokes and only change when the pleopods reverse direction between strokes. Shifts in starting angle and phase create the overall staggered pattern observed among the pleopod pairs. Although the lack of data for PP1 during the recovery-to-power stroke transition (because of obstruction by the walking legs during video analysis) leaves its complete motion pattern unknown, the metachronal wave in the entire system is still evident. Based on the experimental kinematic data for these beating bouts the *Re* of pleopod beating is ~7000, a maximum value calculated specifically for the recovery stroke when the pleopod is moving in the same direction as the body.

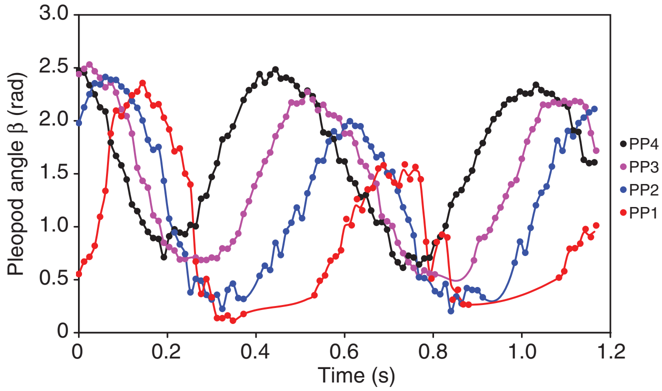

Fig. 4. Time-varying pleopod angle β with respect to the long body axis during a walking sequence with pleopod beating. Solid symbols are the raw data, lines are the interpolated data. Anterior-most pleopod pair is PP1, posterior-most is PP4.

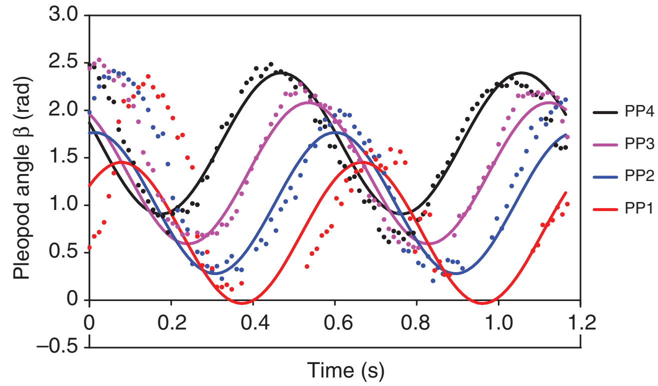

Fig. 5. Pleopod kinematics modelled with a set of simplified trigonometric functions giving pleopod angle as a function of time. Symbols are the original experimental data, lines are the approximating functions.

Modelling pleopod kinematics

We selected the pleopod beating sequence with the most complete kinematic data set (least obstructed by the walking legs) to serve as representative pleopod beating behaviour for further modelling. Spectral analysis of pleopod angle data revealed that a single lower order harmonic, the second harmonic at 1.7 Hz, dominated the motion of the pleopods. This makes up the majority of the signal for all pleopod pairs, accounting for 74% to 86% of the motion pattern of each pleopod. The apparent similarity of the motion patterns for different pleopod pairs allowed the metachronal kinematics of the pleopod system to be modelled with a set of simplified trigonometric functions. The second order harmonic for the PP4 signal served as the basic function from which the functions of the other pleopod pairs were derived. The general expression for a trigonometric function based on a second order harmonic is:

$$\beta(t) = a_0 + a_2 \cos(2pt) + b_2 \sin(2pt)\,, \quad (1)$$

where a and b are Fourier series coefficients with subscripts referring to the specific harmonic, and p is a constant that defines β as a function of time t in seconds. Inserting the appropriate values for PP4 into Eqn 1 yields a simplified expression for pleopod angle as a function of time:

$$\beta(t)_{\mathrm{PP4}} = 1.65 + 0.216 \cos(10.686t) - 0.712 \sin(10.686t)\,. \quad (2)$$

Expressions for PP1 to PP3 were created by applying phase shifts and starting angle shifts to Eqn 2. The phase shift was 0.705 rad, found by multiplying the empirically measured mean (± s.d.) shift along the time axis (0.078±0.003 s) by the mean pleopod angular velocity (9.038±0.484 rad s^{-1}) taken as the slope of the β(t) curve between stroke reversals (maxima and minima). A difference in starting angle of 0.314±0.106 rad between adjacent pleopod pairs was given by the mean shift along the y-axis. The functions for the remaining pleopod pairs are:

$$\beta(t)_{\mathrm{PP3}} = 1.337 + 0.216 \cos(10.686t - 0.705) - 0.712 \sin(10.686t - 0.705)\,, \quad (3)$$

$$\beta(t)_{\mathrm{PP2}} = 1.023 + 0.216 \cos(10.686t - 1.41) - 0.712 \sin(10.686t - 1.41)\,, \quad (4)$$

$$\beta(t)_{\mathrm{PP1}} = 0.709 + 0.216 \cos(10.686t - 2.115) - 0.712 \sin(10.686t - 2.115)\,. \quad (5)$$

The approximating functions and the original experimental data for the four pleopod pairs are plotted in Fig. 5. In addition to simplifying pleopod kinematics, these functions reduce the noise in the original pleopod angle signals. The fit is poor for the first ~0.2 s, a consequence of treating phase and starting angle shifts as constants even though they were computed from averaged experimental data for a behaviour that is highly variable in live lobsters; however, after 0.2 s, the derived functions approximate the motion patterns of the pleopods well. An error analysis showed that the percentage accuracy of the approximating data relative to the experimental data was greater than 93% for PP2 to PP4, but only 83% for PP1 (Table 1); however, the approximating functions for all pleopod pairs had a percentage accuracy higher than 90% when only the angle data collected after the first 0.25 s (nearly halfway into the first beating cycle) were compared. The function for PP1 is also inaccurate in the regions where the angle goes slightly negative, which is not physically possible in a live lobster.

Near-pleopod hydrodynamics

For descriptive purposes only, the flows immediately surrounding the four pleopod pairs (near-pleopod flows) and those behind the last pair and extending back into the surrounding fluid (the wake) are considered separately.

Visualizations of near-pleopod flows revealed that flows around the reciprocating pleopods are unsteady. High-speed flows reaching up to 350 mm s^{-1} between adjacent pleopod pairs develop midway through their power strokes (PP1 and PP2 in Fig. 6A), where flows are either normal to the pleopod surface or have a small downward component. At the same time, a series of clockwise rotating vortices are observed near the ground and anterior to PP1, 2 and 3 (Fig. 6B). Based on the appearance of these vortices just after the pleopods start moving from rest and the accompanying opposite-signed

Table 1. Percentage accuracy of the approximating trigonometric functions of pleopod angle β relative to the original experimental angle data

Pleopod pair	Entire beating sequence	After 0.25 s
PP4	98.1	99.1
PP3	96.7	99.3
PP2	93.4	97.3
PP1	83.2	90.7

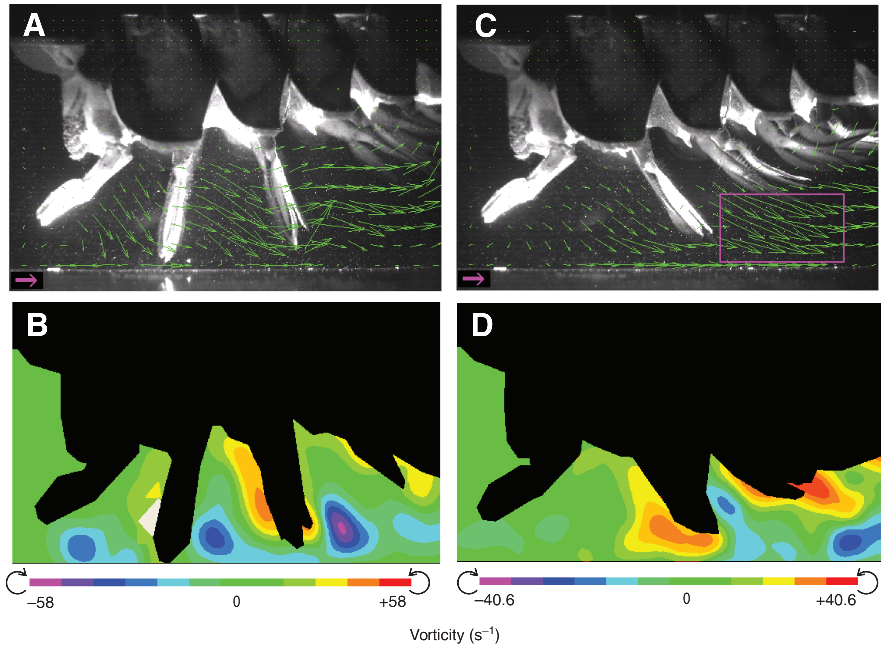

Fig. 6. (A,C) Fluid velocity and (B,D) vorticity fields in the sagittal plane of the mechanical lobster model during the (A,B) middle and (C,D) end of the pleopods's power strokes. Note the different vorticity scales. Reference vector: 100 mm s^{-1}. The boxed region in C is where a small fluid jet with flow velocities up to 380 mm s^{-1} appears between the pleopod tips.

vorticity attached to the pleopod, these appear to be starting vortices; however, the subsequent interaction of the pleopod flows with each other and the ground precludes the opportunity to look for signature flow structures that would confirm that these are starting vortices. Adjacent pleopod pairs approach one another as they complete their power strokes, and this coincides with the appearance of small fluid jets with velocities up to 380 mm s^{-1} between the pleopod tips (boxed region in Fig. 6C) and some shedding of positive vorticity from the pleopods (Fig. 6D).

Although flow fields visualized in the sagittal plane tended to show predominantly rearward flows resulting from the power stroke, the spatial patterns of velocity vectors in the parasagittal planes were more complex and suggested an out-of-plane component of flow in some regions. Relatively slow upward and diverging flows appear around individual pleopods and the spaces between them (Fig. 7A,B), indicating entrainment of fluid toward the pleopods. This is also shown in flow visualizations in the frontal (*xz*) plane just above the ground (Fig. 8). Fluid is drawn upward from the ground as well as downward from beside the body wall of the lobster model to underneath the model, where the pleopods direct it backward as a high-speed bolus of water with flow velocities of 200–300 mm s^{-1}.

Even after the pleopods complete their power strokes, flows remain directed largely rearward until midway through the recovery strokes when sagittal plane flows around the pleopods begin to reverse (Fig. 9A). The vorticity field at this time shows a band of positive vorticity near the ground marking a region of high shear (Fig. 9B). Near-pleopod flows in the sagittal plane have virtually all reversed by the end of the recovery strokes, reaching forward speeds of 150–200 mm s^{-1}.

By contrast, flows in the parasagittal planes do not reverse but remain caudally directed at speeds of 60–180 mm s^{-1} throughout the pleopod recovery strokes, diminishing slightly at the end of the stroke (Fig. 10A). Consistent with this observation, the frontal plane flow field at the end of the recovery strokes revealed that flow reversal is indeed largely confined to the sagittal plane and only in the region immediately surrounding the pleopods (Fig. 10B). The near-pleopod flows from the mechanical lobster model indicate continual entrainment of fluid from the sides and front of the model and direction of this fluid backward. The power stroke and recovery stroke flow patterns described above repeat throughout the mechanical model's eight-cycle beating bout, with the spatial patterns showing little variability among different beat cycles. The unsteady flows thus appear to have a cyclic time-varying character.

Pleopod wake development

Viewed in the sagittal plane of the lobster model, fluid flow posterior to the last pleopod pair is initially angled down approximately 35 deg. from the horizontal at a speed of ~75 mm s^{-1}, and then impinges upon the ground under the tail fan (Fig. 11). Growth in the size and strength of the pleopod jet wake occurs over the first two beat cycles in the beating bout. A time-series of flow fields from the frontal plane shows how the jet expands backward and laterally (Fig. 12). Directly behind the lobster model, a small region of high-speed flows first appears after the power strokes. This rapidly moving fluid propagates away from the model, while subsequent power strokes add to the developing wake. The general temporal trend is the appearance of a region of high-speed flow within the wake per complete power stroke and with little flow reduction during the recovery strokes. By the end of the fourth power stroke (3.5 cycles), the jet has extended back a distance at least four times the mean pleopod length, and sagittal plane flow fields show that the flow is predominantly parallel to the ground (Fig. 13A). The gross wake morphology changes little an additional four beat cycles later, suggesting that the jet is fully established (Fig. 13B). Fluid velocities within the pleopod jet wake reach up to 340 mm s^{-1}, and elongated bands of opposite-signed vorticity indicate regions of high shear at the edges of the jet (Fig. 13C).

Fluid velocity data were extracted from the PIV flow maps to compare flow velocities in two locations of the pleopod jet wake: 45 mm ('proximal') and 108 mm ('distal') from the last pleopod pair (Fig. 14). Data from points located on the line where the frontal and sagittal planes intersect were plotted against time to gain a general understanding of how the wake flow varies over the course of a beating bout. In the proximal wake location immediately behind

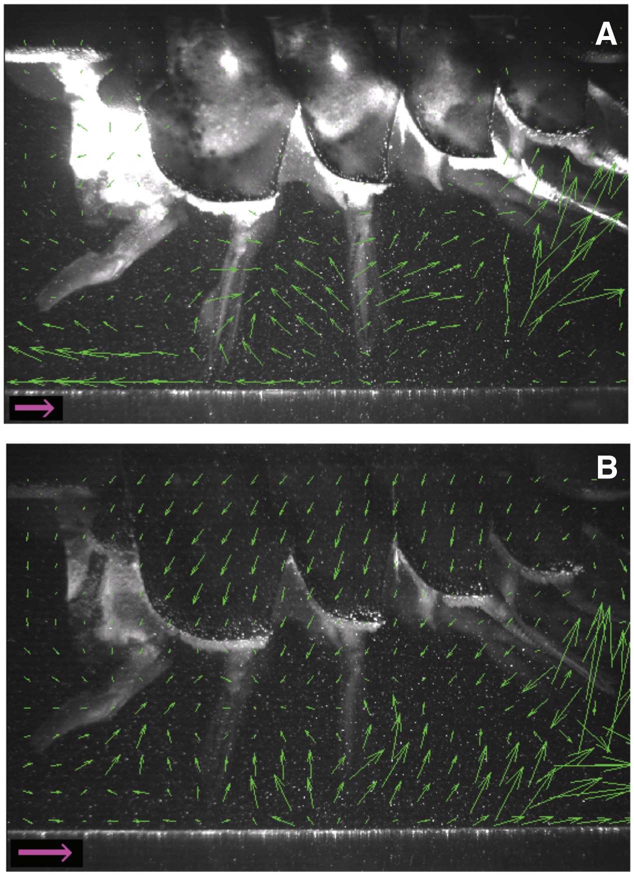

Fig. 7. Flows in a parasagittal plane (A) 20 mm and (B) 30 mm left of sagittal where pleopods are midway through their power strokes. Entrained (into-the-page) flows are suggested by downward flows from beside the body wall of the model and upward flows from the ground toward the pleopods Reference vector: 50 mm s^{-1}.

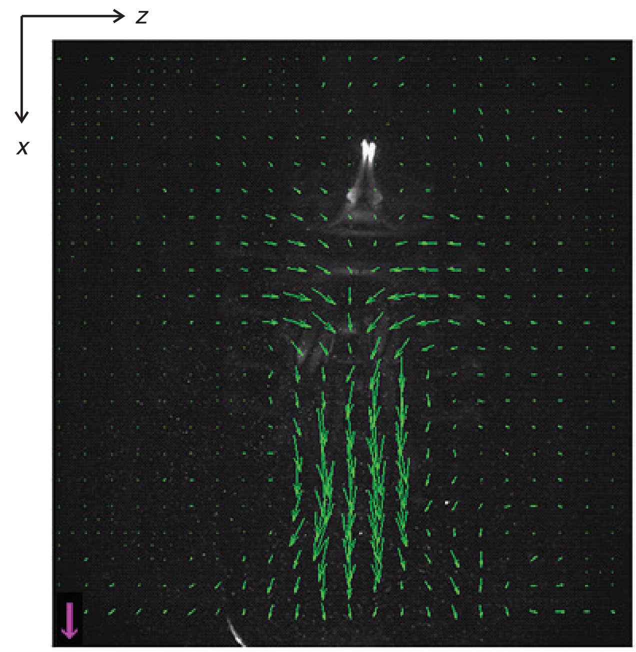

Fig. 8. Near-pleopod flows visualized in a horizontal (frontal, *xz*) plane with anterior at top. Fluid is being drawn under the lobster model toward the sagittal plane and directed caudally. The pleopods are folded up against the ventral abdomen after completing a power stroke. The bright spot near the top is the male's modified, non-paddling pleopod pair. Reference vector: 100 mm s^{-1}.

the pleopods, fluid velocities are unsteady and oscillate at a frequency of ~1.3 Hz (Fig. 15, red line), equal to the pleopod beat frequency. This matching of frequencies is a result that has been previously observed (Davis, 1968a). Just posterior to the tail fan in the distal wake, however, fluid velocities initially increase and then begin to stabilize with only small oscillations in local fluid velocity about a velocity of ~100 mm s^{-1} (Fig. 15, black line). The jet maintains its rearward direction throughout the entire beating bout, indicated by the positive fluid velocities.

Fluid velocity profiles from the proximal and distal locations in the jet wake show the increase in the jet velocity and span over the period of development (Fig. 16A). After the jet has been fully established, mean velocity profiles from the frontal and sagittal planes illustrate that flow velocities in the distal wake position have relatively small deviations about the mean, compared with those about the mean from the proximal wake location (Fig. 16B, Fig. 17A). Fluid velocities are particularly variable near the jet core and the ground. Parasagittal plane flows are less strongly oriented rearward at the jet core, and even exhibit some reversal (negative velocities) close to the pleopods (Fig. 17B,C). This probably corresponds to out-of-plane flows similar to those apparent from visualizations of near-pleopod flows in the parasagittal planes (Fig. 7). In addition, the amount of deviation in flow velocities from the mean profiles in the parasagittal planes is similar for the proximal and distal wake positions. The mean velocity profile from the outermost parasagittal plane further downstream from the pleopods is actually greater than the profile from directly posterior to the pleopods (Fig. 17C), reflecting lateral expansion of the jet as it extends backward.

Quantifying pleopod fluid force

Pleopod thrust was calculated using a simplified equation for steady jet thrust that is based on the rate of change of fluid momentum (Vogel, 2003), and given by:

$$T = \rho A_j u_j^2 \,, \qquad (6)$$

where ρ is the fluid density, A_j is the cross-sectional area of the jet, and u_j is the component of jet velocity normal to the wake's transverse (*yz*) plane (Anderson and Grosenbaugh, 2005), or in other words, the component of velocity parallel to the long axis of the lobster model. Using this component yields a force that represents only forward thrust and ignores any lateral forces. Assumptions for this equation include steady flow that is normal to and uniform across the transverse plane, and that flows are not in a velocity gradient.

The cross-sectional shape of the jet was estimated by combining information from fluid velocity profiles in the multiple image planes. The height of the jet is approximately 60 mm in the sagittal plane, and its width is approximately 60 mm in the frontal plane that is 16.5 mm above the ground. Parasagittal velocity profiles indicate that jet velocity and height decrease with increasing lateral distance from the sagittal plane. Modifying the standard assumption of a circular cross section to fit the measurements of jet width and height measured in the frontal and sagittal planes, the pleopod jet's cross-sectional shape was approximated as a half-ellipse with a 60 mm major radius and 30 mm minor radius.

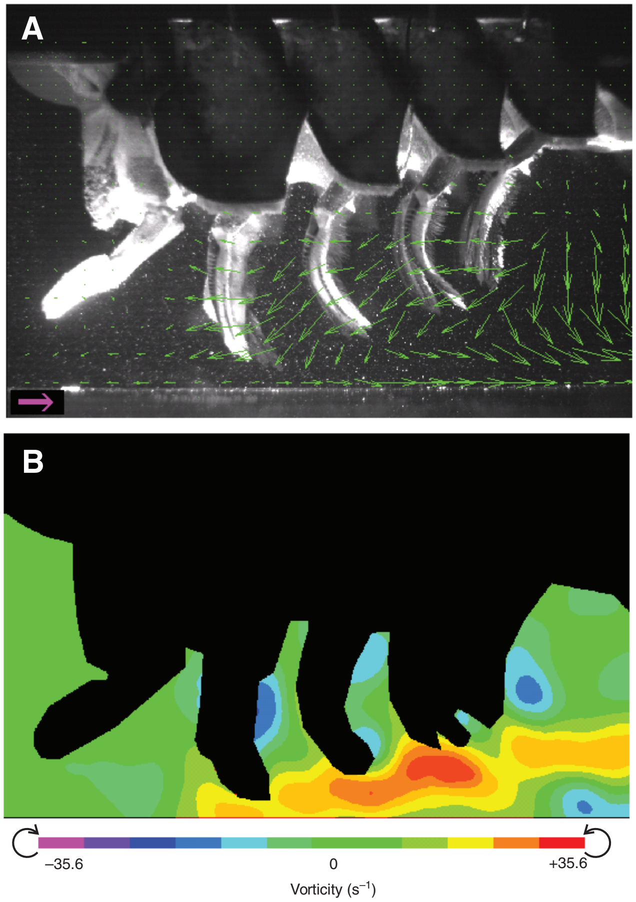

Fig. 9. (A) Fluid velocity and (B) vorticity fields in the sagittal plane of the mechanical lobster model during the middle of the pleopods's recovery strokes. Reference vector: 100 mm s^{-1}.

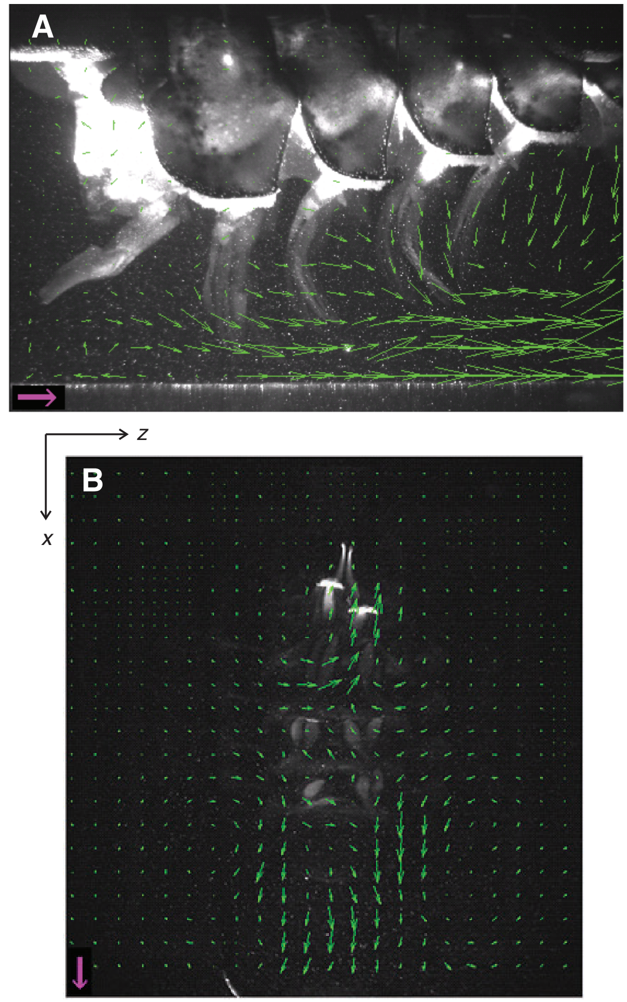

Fig. 10. (A) Flows in the parasagittal plane 20 mm left of sagittal are still rearward during the middle of the pleopods's recovery strokes. Reference vector: 50 mm s^{-1}. (B) Recovery stroke flows visualized in the frontal plane with anterior at top. Forward flows are mostly confined to the sagittal plane. Reference vector: 100 mm s^{-1}.

Velocity profile data from the distal position in the wake in the sagittal plane were used to calculate jet thrust. Flows at this location in the wake were largely normal to the transverse plane, but had not experienced significant decline caused by fluid viscosity. The plot of wake flow velocity over time (Fig. 15) demonstrates that distal wake velocities are still within the range of those in the proximal wake position. Although these time-series velocity data do not fulfil the model's assumptions of a uniform and steady flow field, for the purposes of providing a first-approximation of lobster pleopod fluid force we use a spatially and temporally averaged jet velocity. Mean jet thrust was calculated using the average jet velocity across the jet diameter (N=20 velocity data points) for each flow visualization during the period in which the jet was fully developed (N=20 visualizations). At jet velocities of 98±29 mm s^{-1} (mean ± s.d.), mean thrust in the direction of the jet axis is 27 mN. The time-averaged maximum jet velocity during steady conditions (N=20 visualizations) was 138 mm s^{-1}, yielding a maximum pleopod thrust of 54 mN.

DISCUSSION

In this paper we determine the kinematics of *in vivo* pleopod beating in the lobster *Homarus americanus* and subsequently model the motion patterns of the multi-paddle system with a set of simple trigonometric functions that approximate pleopod kinematics. We use these functions to prescribe pleopod motion patterns for a mechanical lobster model and visualize the surrounding flow field of the operating model. The model's wake is quantified to provide an estimate of pleopod thrust.

Typical values observed here for kinematic quantities that characterize the pleopods's metachronal pattern, such as beat frequency, angular velocity and phase shifts among adjacent pleopod pairs, were consistent with descriptions of pleopod kinematics for *H. americanus* in the numerous studies by Davis (Davis, 1968a; Davis, 1968c; Davis, 1969). The beat frequencies observed in the particular lobsters analyzed in this study ranged from 1.3 Hz in the largest lobster to 2.3 Hz in the smallest lobster, during routine forward walking. These values agree with a mean beat frequency of 1.8 Hz reported by (Davis, 1968c), who also found that frequency was highly variable within individual lobsters. Though the data resolution in this study is insufficient to suggest the nature of the relationship between pleopod beat frequency and body size, negative relationships between limb beat frequency and body length have been reported for other paddling crustaceans, such as krill (Thomasson et al., 2003), shrimp (Frank and Widder, 1994) and isopods (Ellenby, 1951).

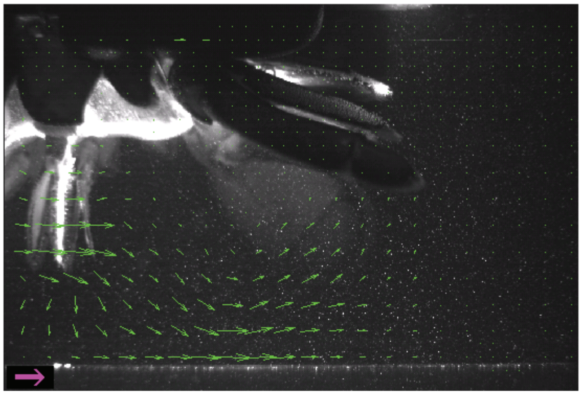

Fig. 11. Pleopod wake flows in the sagittal plane of the mechanical lobster model at the start of a beating bout. The last pleopod pair is in mid-power stroke. The initial flow is directed down and backward, impinging upon the ground. Reference vector: 100 mm s^{-1}.

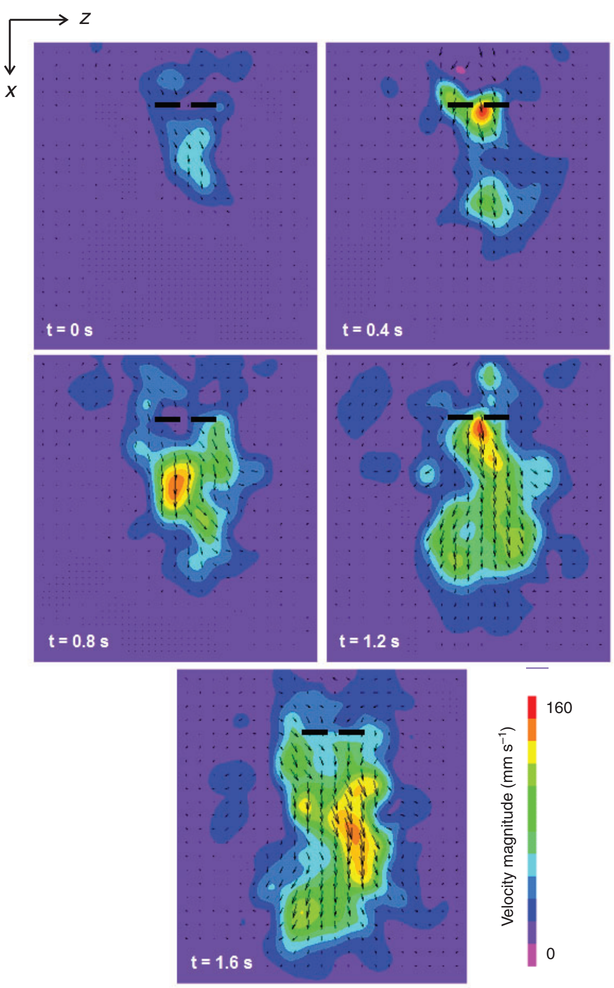

Fig. 12. The growth of the pleopod jet wake depicted in a time-series of frontal plane flow velocity vector fields viewed from underneath a mechanical lobster model, spanning two complete pleopod beat cycles (beat frequency 1.3 Hz). Anterior is at the top; the bold black bars indicate the location where the last (fourth) pleopod pair articulates with the abdomen. Velocity vector magnitude is colour-coded, red marking the regions with the highest flow speeds.

Metachronal kinematics in live lobsters

Metachronal patterns are ubiquitous in multi-limbed systems. They appear in the motion of pleopods on crayfish (Copp and Hodes, 2001), burrowing shrimp (Stamhuis and Videler, 1998a) and krill (Kils, 1981; Yen et al., 2003), and the feeding appendages and swimming legs on copepods (van Duren and Videler, 2003). Outside the Crustacea, metachronal rhythms are used for locomotion by the comb plates on ctenophores (Barlow et al., 1993), flagella on protozoa and parapodia of walking clam worms (Sleigh and Barlow, 1980). In their review on metachonal systems in animals, Sleigh and Barlow (Sleigh and Barlow, 1980) proposed that the function of the coordinated movements in these systems is to allow each limb to carry out its motion pattern unobstructed by adjacent limbs, while the whole system exploits a synergistic effect from the multiple limbs working simultaneously.

The lobster pleopod system displays a clear metachronal pattern with regular phase shifts and starting angle shifts between the pleopod pairs (Figs 4 and 5). This kinematic pattern is shared by other crustaceans that span a few orders of magnitude in size and Reynolds number. The swimming legs in the small (~1 mm body length) copepod *Temora longicornis* move in a pattern that closely resembles lobster pleopod kinematics but operate at a *Re* of 30–100 during escape behaviours (van Duren and Videler, 2003). Reynolds numbers that are more comparable to that for the American lobster reported in this study are associated with the swimming appendages of larger copepods (Yen and Strickler, 1996) and amphipods (Boudrias, 2002). Both copepod swimming legs and amphipod pleopods move metachronally during their power strokes, but have entirely synchronous recovery strokes (Boudrias, 2002; van Duren and Videler, 2003). The four pairs of lobster pleopods do not perform their recovery strokes in complete synchrony but do display a tendency to group together as a result of the shifts in phase and starting angles. Departure from a fully metachronal sequence may have hydrodynamic consequences that increase the overall performance of a multi-limbed system (Morris et al., 1985; van Duren and Videler, 2003), as evidenced by the flow visualizations presented in this paper.

Using our experimental kinematic data, we derived a set of trigonometric functions for pleopod angle over time, $\beta(t)$, from a single basic equation to which we applied shifts in phase and starting angle. Overall, these functions closely approximated pleopod beating in live lobsters. The poor fit between the modelled data and the experimental data at the start of the beating bout may be explained by an abrupt change in pleopod beat frequency by the lobster. The negative angles predicted by the approximating function of PP1 are also instances where the model is incorrect. The value for β at the extreme anterior position of PP1 are unknown, but it is clear that the actual curve of $\beta(t)$ for PP1 will have a motion pattern that departs from the simple periodic pattern displayed by the other pleopod pairs. What is the reason, then, for not developing specific functions for each pleopod pair? Independently derived equations may have little influence on the shape of the curve, but the ability to model the pleopod system with a general function and slightly modified versions of it has implications for the degree of simplicity in the neuromuscular control of the system in a live lobster.

The hydrodynamics of metachrony

The motor-driven model built from the exoskeleton of a real lobster performed a simplified version of the pleopod motion patterns found in live lobsters. Differences between the power and recovery strokes in the configuration of each pleopod's articulating rami arose solely by a passive drag-assisted mechanism, whereas in a live lobster, muscle-mediated spreading and bending are likely to augment the asymmetry further. Although this may result in altered flow patterns, the mechanical lobster model was still able to simulate the metachronal wave found in live lobster pleopod beating.

We used the quantitative flow visualization technique of particle image velocimetry to characterize pleopod flow structure and to measure the mechanical forces that the model's oscillating pleopods generate. Combining information from flow visualizations in orthogonal planes revealed that over the course of approximately eight pleopod beat cycles performed by the mechanical lobster model, the pleopods continuously entrain fluid from the sides and front of the model and accelerate it posteriorly. Near-pleopod flows exhibit unsteady dynamics as the appendages execute their periodic pattern of alternating power and recovery strokes. The wake develops into a strong rearward jet whose dynamics in close proximity to the pleopods are also unsteady, approaching a steadier condition further downstream. For ease of description in the Results, near-pleopod flows and wake flows were treated separately; here, the observed flows around the pleopods and in their wake are considered together with pleopod kinematics to propose a synthesized interpretation of pleopod hydrodynamics during a beating bout.

Rhythmic pleopod beating creates high-velocity flows (and associated lower relative pressure) under the abdomen, which help to continuously entrain more fluid toward the pleopods. Their adlocomotory metachronal beating pattern – where cycles begin at the last pleopod pair and are separated by phase delays as they proceed to the first pair – allows each pair to initially operate as a paddle unimpeded by its neighbours (Sleigh and Barlow, 1980). The development of high velocity flows directly behind each pleopod during its power stroke (Fig. 6A) suggests that a pleopod can accelerate its added mass of water with little interference from the posterior pleopod pair. We propose that one potential thrust-producing mechanism that could be exploited at the beginning of this metachronal sequence is delayed stall (Dickinson, 1996). An extended pleopod beginning its power stroke is effectively a foil at a large angle of attack, the upper edges of the splayed-out rami forming the leading edge. The positive vorticity observed at the anterior face of the pleopods during the power strokes (Fig. 6B,D) may represent an attached leading edge vortex. The low pressure associated with this vortex results in a normal transient force whose horizontal component is forward thrust (Dickinson, 1996). The unsteady force arising from this so-called 'impulsive start' diminishes as flows approach steady state conditions, and so would be especially important for oscillating pleopods that travel only a short distance before they change their angle of attack and reverse direction (Dickinson, 1996). Higher resolution PIV can be used in future experiments to look for an attached leading edge vortex at the dorsal edges of the pleopod rami.

Metachrony can similarly be beneficial for the generation of drag-based thrust as the pleopods progress through their power stroke arc, as this force is proportional to projected area and is maximal when a pleopod is oriented perpendicular to the long body axis and the oncoming flow. As the pleopod pairs sweep through this point in succession, each generates its own force that contributes to the

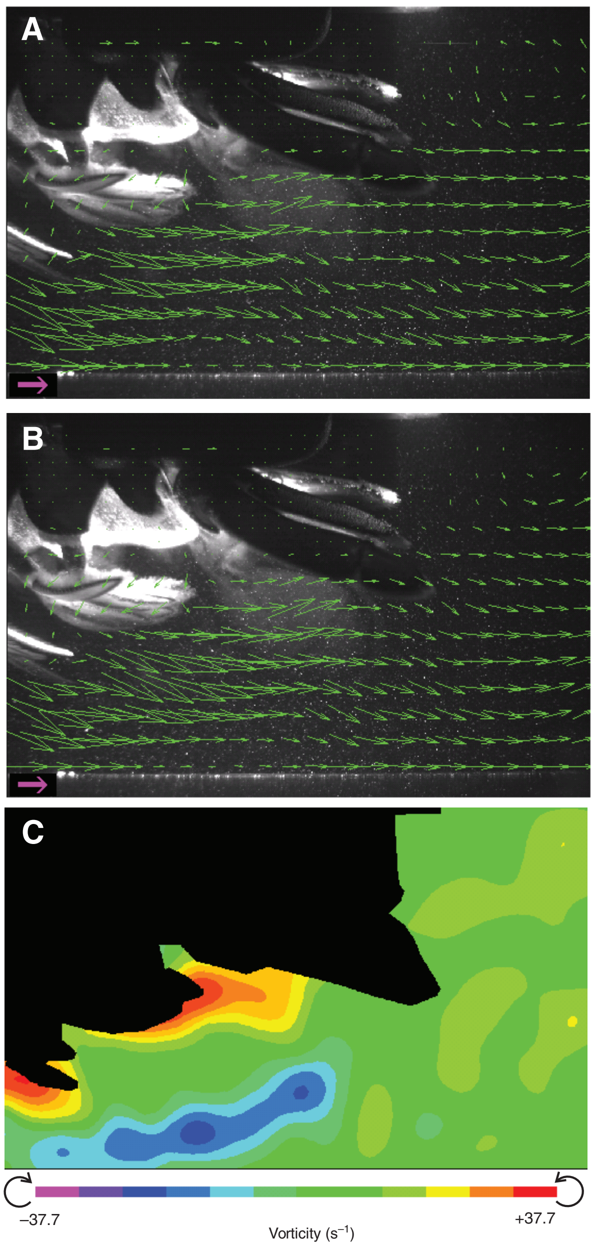

Fig. 13. The pleopod wake visualized in the sagittal plane of the lobster model. (A) After the fourth power stroke, wake flow is predominantly parallel to the ground in the established jet, whose structure is constant another four cycles later (B). Reference vector: 100 mm s^{-1}. (C) Elongated bands of vorticity indicate high shear at the edges of the pleopod jet.

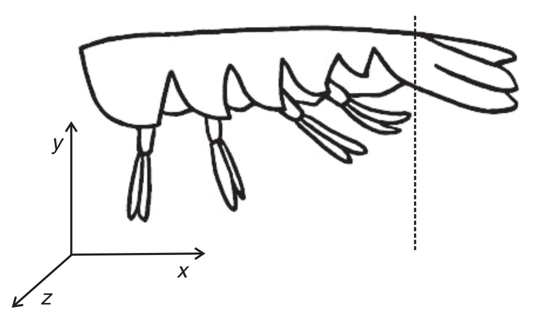

Fig. 14. Schematic diagram of the locations (broken lines) in the pleopod wake where fluid velocities were compared. The location immediately posterior to the pleopods under the tail fan is referred to as the 'proximal' position, and the location further downstream past the tail fan is referred to as the 'distal' position. The axes indicate the coordinate system used.

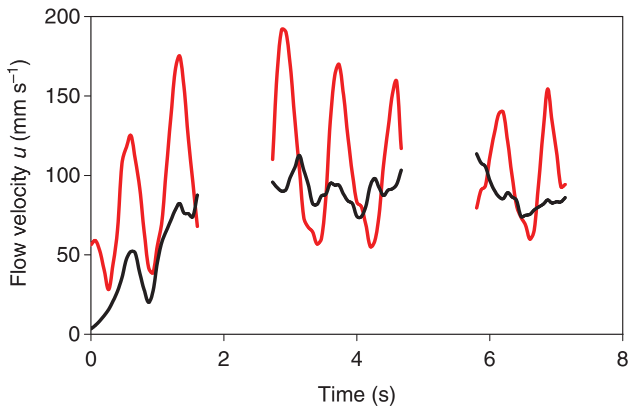

Fig. 15. Pleopod jet velocities at a proximal position in the wake immediately behind the last pleopod pair (red line) are unsteady throughout a beating bout, whereas velocities further downstream at the distal position (black line) become steadier, with only small oscillations. The rearward direction of the jet is maintained during the entire bout (*u*>0). Data are from points located in the line where the frontal and sagittal planes intersect; the gaps are periods where no data were collected. A three-point running average is plotted to reduce noise.

total thrust of the system. If each pleopod pair makes use of these phenomena early in its power stroke, they should be able to collectively generate more thrust than they would if beating synchronously. The mechanical lobster model may be used in future experiments to confirm that a metachronal pattern results in greater thrust production than a synchronous one. Modelling may inform whether the benefit outweighs any associated increases in energetic (muscular) cost to the pleopods.

Evidence for interaction between different pleopod pairs late in their power strokes appears as small inter-pleopod fluid jets (Fig. 6C). Lochhead (Lochhead, 1977) postulated that the spaces between pleopods could function as pumps, where periodic changes in volume and pressure entrain and expel fluid alternately. Barlow et al. (Barlow et al., 1993) similarly proposed a 'pump' model after visualizing fluid jets emerging from between the rectangular paddle-shaped comb plates on the ctenophore *Pleurobrachia pileus*. The results of the present study support such a pump model for lobster pleopods. Flow speeds within these jets were typically faster than pleopod tip speeds, suggesting that they are indeed caused by pleopod pairs coming together and squeezing fluid out from between them.

As the pleopods reverse direction and make their recovery strokes, mechanisms within each pleopod and within the entire system appear to minimize any opposing effects caused by their forward motion. Drag causes the pleopod to bend at its internal joint and its rami to overlap, decreasing the total projected area of the pleopod. Active collapse of the pleopods in live lobsters probably reduces the opposing drag of the recovery stroke even further. In addition, as a consequence of the system's kinematics where the pleopods tend to physically group together during their recovery strokes compared with the more spatially staggered power strokes (Fig. 4), the opposing drag on the pleopod set may be closer to that for a single pair of pleopods (Morris et al., 1985). This change in pleopod configuration may explain how the rearward flows established during the power stroke are maintained at the sides of the lobster model during the recovery stroke (Fig. 10A,B). PIV analysis of the ventilation current from the pleopods of tube-dwelling mud shrimp (*Callianassa subterranea*) has similarly shown that flow velocities are minimally affected by the recovery strokes of articulating appendages beating with a metachronal pattern (Stamhuis and Videler, 1998c).

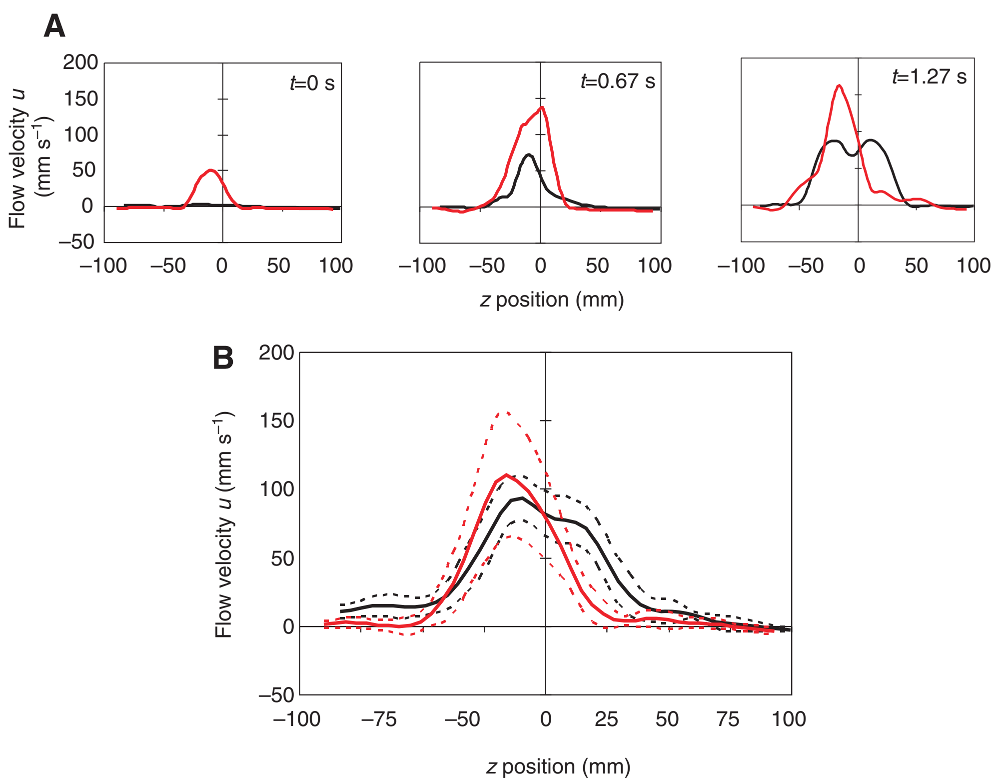

Fig. 16. (A) Velocity (*u* component) profiles at selected times during the development of the pleopod jet wake in a horizontal plane (~16.5 mm above the ground). (B) Time-averaged velocity profile of the established jet (*t*>2.73 s). Red lines represent profiles from the proximal wake position; black lines represent profiles from the distal wake position. For B only, solid lines: mean profile; broken lines: ±s.d.; *N*=51.

The forward flows that the pleopods do induce are typically 80 mm s^{-1}, considerably slower than power stroke-generated flows, and are mostly confined to the sagittal plane and the region immediately around the pleopods (Fig. 9A, Fig. 10B) as they carry along their added mass. These results suggest that opposing forces associated with forward flows on the recovery stroke are relatively small compared with the thrust generated from the power stroke. Furthermore, these forward flows around the pleopods may actually contribute to forward thrust *via* another unsteady mechanism. Nauwelaerts et al. (Nauwelaerts et al., 2005) observed similar flow patterns around frog feet that were dragging water along with them during their return strokes. They proposed that the deceleration of this entrained water as the foot completes its return stroke and increases its projected area results in an acceleration reaction force that contributes to forward thrust even before the legs begin extending in their backward kick. A lobster pleopod could similarly experience this unsteady force as it changes over from its recovery to a power stroke.

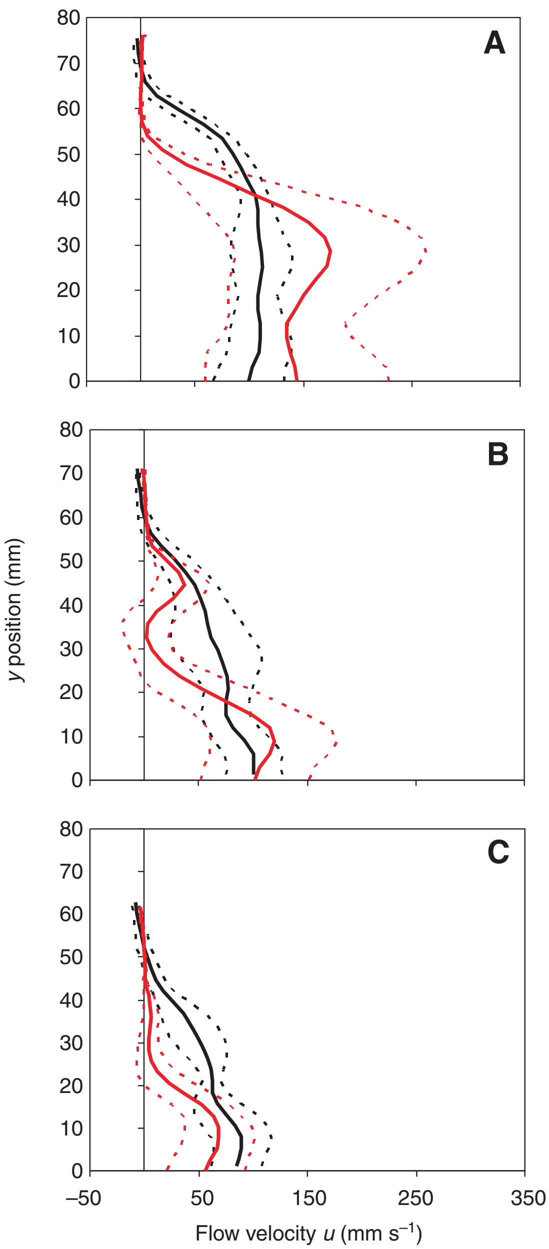

Fig. 17. Time-averaged velocity (u component) profile of the established pleopod jet wake in (A) the sagittal plane, (B) the parasagittal plane 20 mm left of sagittal, and (C) parasagittal plane 30 mm left of sagittal for the mechanical lobster model. Red lines represent profiles from the proximal wake position, black lines represent profiles from the distal wake position (solid lines: mean profile; broken lines: ±s.d.; N=20 for each mean profile).

The combined effects of each pleopod pair and their interactions within this metachronal system create a fast-moving mass of water that propagates backward and slightly downward, resulting in initial wake flows that impinge on the ground (Fig. 11). With each consecutive beat cycle, additional fluid masses are sent backward and contribute to the developing wake. These high-speed masses of fluid are responsible for the unsteady flow velocities observed immediately behind the pleopods during a beating bout, particularly in the sagittal plane (Fig. 15, red curve; Fig. 17A). But moving downstream, the flows become integrated with the background wake flow and fluid velocities approach a steadier state (Fig. 15, black curve). The result of rhythmic pleopod beating is a continuous fluid jet oriented parallel to the substratum, with the reaction force of the rearward jet flow being forward thrust. We propose that asymmetrical strokes within a beat cycle and a metachronal beating pattern help maintain the jet's continuous flow and reduce the amplitude of oscillatory flows in the wake compared with synchronous strokes. Consistent with this hypothesis, previous research has shown that metachronal kinematics help to prevent energetically expensive pulsatile (unsteady) flows within the tube-shaped burrows of mud shrimp that use pleopods to generate ventilation currents (Stamhuis and Videler, 1998c).

The propulsive jets that many animals produce are often a part of a vortex ring structure shed by oscillating foils [e.g. fish pectoral fins (Drucker and Lauder, 1999; Drucker and Lauder, 2000); frog feet (Stamhuis and Nauwelaerts, 2005)]; however, velocity and vorticity fields in the lobster's near-pleopod and wake flows did not clearly indicate a vortex wake, suggesting that the ground surface and the close approach of pleopods as they complete their power strokes cause flows to interact and ultimately hinder the formation of distinct fluid structures. Instead, parallel bands of opposite-signed vorticity probably represent high shear layers at the edges of an elongated jet (Fig. 9B, Fig. 13C) (Anderson and Grosenbaugh, 2005; Yen et al., 2003). Elongated jets have been identified in a pelagic relative of the lobster, the krill *Euphausia pacifica* (Yen et al., 2003), and although not arising by the same mechanism, swimming squid (*Loligo pealei*) have also been shown to create elongated jet wakes (Anderson and Grosenbaugh, 2005).

This paper presents new information on how the pleopods of the American lobster interact with the surrounding fluid to generate force, and can also offer insight into the mechanics of pleopods and multi-limb systems in other malacostracan crustaceans. Pleopod morphology varies greatly among crustacean taxa, but the specialization of pleopods for swimming has evolved many times in both benthic and pelagic groups (McLaughlin, 1982). Pleopods used for swimming can be slender and feathery (as in amphipods, shrimp, some crayfish); 'ovate' or paddle-shaped (clawed lobsters, isopods, stomatopods); or can form a functionally single broad paddle using an *appendix internae*, a structure that physically connects the left and right pleopods together (tanaids) (McLaughlin, 1982). Despite having a Reynolds number (*Re*) differing by up to several orders of magnitude from a lobster, it has been shown that crayfish (Breithaupt and Ayers, 1998), euphausid krill (Kils, 1981; Yen et al., 2003), and calanoid copepods (van Duren and Videler, 2003) also use metachronally beating limbs to entrain fluid and produce jet-like flow as a mechanism of propulsion.

The mechanical lobster model that we developed can easily be modified to test functional hypotheses in other animals. Removing the ground surface, building a scaled-up model that is dynamically similar to the real animal (Koehl, 2003), and changing appendage morphology or kinematics are all ways to adapt our motor-driven physical model so that it can be used to explore the hydrodynamics of other multi-limb systems in crustaceans and beyond.

Additional future experiments with the mechanical lobster model should incorporate forward motion of the model to learn how the hydrodynamics change with body movement. Catton et al. (Catton et al., 2007) showed that flow morphology and velocity differed between free-swimming and tethered copepods in such a way that simply mathematically adding a background free-stream flow could not reproduce the free-swimming flow field. Similar to the copepods in the experiments of Catton et al. (Catton et al., 2007), we predict that with a lobster body's forward travel, the pleopod wake will narrow. Also, flow velocities in the region directly ventral to the copepod body are slightly higher in magnitude in the free-swimming animals (Catton et al., 2007); if this also occurred in the lobster, there is potential for greater jet thrust.

Testing whether any sexual dimorphism in abdominal or pleopod morphology affects the hydrodynamics is also possible with the mechanical lobster model. MacCormack and DeMont (MacCormack and DeMont, 2003) reported differences in the scaling relationship between abdomen area and body size in male and female *H. americanus*, and the pleopods of reproductive females tend to have longer setae that would increase their effective paddling area (Talbot and Helluy, 1995).

Pleopod thrust

Complex spatial and temporal patterns of fluid flow near the lobster's oscillating pleopods can make quantifying their hydrodynamics a challenge; however, the observation that the wake flows are considerably steadier permits one to simplify the situation. Assuming that the fully developed pleopod jet wake approximates steady state conditions, attention can be focused on the wake to estimate the amount of force exerted by all of the pleopods. The effects of interactions among the pleopods are inherently included in this analysis.

The present analysis of the jet revealed that a large lobster's oscillating pleopods can generate a mean thrust of 27 mN and peak thrust of 54 mN. The simplified equation used to calculate pleopod thrust assumes that the jet flow is steady (Anderson and Grosenbaugh, 2005). A so-called quasi-steady analysis is applied when the time-averaged values of unsteady quantities are entered into an equation for steady flow (Anderson and DeMont, 2000; Daniel, 1984). Our use of spatially and temporally averaged flow velocity data in the jet thrust model ignores unsteady effects, providing an approximation of average pleopod thrust. Our rationale for using a quasi-steady analysis was based on the observation that wake flows just downstream of the lobster model approached nearly steady conditions after the jet had been fully established. The relatively small deviations observed around time-averaged velocity profiles from the distal wake position in the established jet (Fig. 16B, Fig. 17) also support this claim. The assumption of flow direction oriented normal to the transverse plane of the wake was assessed by comparing profiles of the total jet velocity to profiles of only the component of velocity normal to the transverse plane. For the majority of the established jet flow visualizations in the sagittal and frontal planes, the two velocity profiles exhibited similar overall shapes and flow speeds. Flows parallel to the transverse plane were therefore assumed to be negligible, and were ignored by using only the *u*-component velocity to calculate jet thrust. Assumptions that flows were not in a velocity gradient but uniform across the cross-sectional area of the jet were more tenuous given the presence of shear flow and the proximity of the ground. Velocity was averaged across the jet diameter to approximate uniform flow, but a more exact method would involve measuring fluid velocities in additional parallel and perpendicular planes to obtain a higher resolution of flow velocities in space (Vogel, 2003). Forces for an array of small areas (dA) in the transverse plane, where uniform flow would be required only across dA, could be computed and integrated over the entire area (A) to gain a more precise measurement of pleopod force (Vogel, 2003). Future work on pleopod mechanics can provide higher resolution data to examine the unsteady dynamics of the pleopod wake and the consequences for thrust production.

For comparison of the thrust computed from the steady jet equation with force calculated from another method, the drag force on a flat plate oriented normal to flow was calculated as an estimate of pleopod force using the equation:

$$D = 0.5\rho A_{pp} U_{pp}^2 C_d\,, \quad (7)$$

where D is the drag, A_{pp} is the pleopod projected area (averaged over the four pleopod pairs, 880 mm^2), U_{pp} is the relative speed between the pleopod and fluid, approximated as the pleopod velocity at the midpoint of the rami (presumably the main paddling elements; 170 mm s^{-1}), and C_d is the coefficient of drag (Vogel, 1994). C_d was based on plate width and given by the equation:

$$C_d = 1.17 + 17.1\,Re^{-1.21}\,, \quad (8)$$

with Re=7500 (Stamhuis and Videler, 1998c). The drag force summed for four pleopod pairs is ~60 mN, which agrees with the maximum force calculated from the steady jet thrust equation. But because the equation for jet thrust is particularly sensitive to changes in jet velocity (Eqn 1), and results were obtained using representative models of lobster morphology and kinematics, the reported thrust values should be viewed as insight into the order of magnitude of the forces that lobster pleopods can generate.

Jet-assisted walking in lobsters

The American lobster's pleopod forces are comparable to the thrust generated by some well-known proficient swimmers such as bluegill sunfish (*Lepomis macrochirus*) and surfperch (*Embiotoca jacksoni*) swimming at slow to moderate speeds using their pectoral fins (Drucker and Lauder, 1999; Drucker and Lauder, 2000), and squid (*Loligo pealei*) using jet propulsion (Anderson and DeMont, 2000; Anderson and Grosenbaugh, 2005) (Table 2). How pleopod forces compare with walking forces was not addressed in this study, but insight into their relative contribution to forward propulsion is gained by noting that pleopod forces are an order of magnitude smaller than the maximal force exerted by the fourth walking leg in *H. americanus* (Mitchell and DeMont, 2004). Another way of assessing the potential contribution of pleopod thrust to locomotion is to compare them to the range of maximum forces exerted by a variety of animals, reported by Alexander (Alexander, 1985). Maximum force per body weight plotted against body mass for animals generating force from several kinds of processes in both air and water (e.g. flying, swimming, biting, jumping) tended to lie between two lines defined by (0.5 body mass$^{-1/3}$) and (20 body mass$^{-1/3}$). Pleopod thrust that reaches a maximum of 0.054 N in a 1.2 kg lobster falls far short of the lower bound. This result along with the comparatively small

Table 2. Summary of the thrust forces generated by the lobster *Homarus americanus* and other aquatic species

Species	Approx. body size (mm)	Approx. velocity (body lengths s^{-1})	Mean thrust (mN)	Source
American lobster (*Homarus americanus*)	236	–	27	This study
Squid (*Loligo pealei*)	320	0.8	30	Anderson and DeMont, 2000
Bluegill sunfish (*Lepomis macrochirus*)	200	0.5	11*	Drucker and Lauder, 1999
		>1.0	35*	Drucker and Lauder, 2000
Surfperch (*Embiotoca jacksoni*)	210	0.5	26*	Drucker and Lauder, 2000
Leopard frog (*Rana pipiens*)	–	–	71*	Johansson and Lauder, 2004
Copepod (*Pleuromamma xiphias*)	<10	–	0.25	Morris et al., 1985

*Thrust per stride.

magnitude of pleopod force relative to those from the walking legs, suggest that the pleopods are a supplementary source of thrust. Considering the competing demands from the pleopods's multiple functions in lobsters, they may not have been under strong selective pressure to be optimized for locomotory performance. Although the relative contribution of pleopod forces to total propulsive force from adult lobsters is unknown, the results of the present study suggest that the pleopods are at least capable of generating enough force to contribute to locomotion.

We propose that lobster pleopods could function in a jet-assisted walking mechanism, where the pleopod jet flow assists the legs in forward propulsion. Besides being the main source of propulsive force, the walking legs could function to control the characteristics of the pleopod jet by adjusting the space between the body and the ground. This dual component system of multiple paddles behind a set of walking legs is seemingly only found in decapod crustaceans. A jet-assisted walking mechanism may be especially important to lobsters that occupy habitats with particularly rocky bottoms, or those that undergo seasonal long-distance migrations.

Though not directly tested here, whether pleopod flows can function in stabilization mechanisms in *H. americanus* also merits further study. The relatively low pressure under the abdomen that draws fluid toward the pleopods might also help lobsters withstand strong benthic currents and surge (Ayers, 2004). Several species of crayfish have been shown to adopt body postures that would result in downward-directed stabilizing forces when faced with fast oncoming currents (Maude and Williams, 1983). Vigorous pleopod beating often accompanied this posture shift, but the maximum current speed that the crayfish could tolerate appeared to be unaffected by surgical removal of the pleopods (Maude and Williams, 1983); however, the slender shape of crayfish pleopods (Copp and Hodes, 2001) may limit their ability to generate flows of comparable velocity to those now reported for the wider, paddle-shaped pleopods on *H. americanus*.

Conclusions

The presence of multiple paddles and their metachronal kinematics appear to have advantageous mechanical consequences for the American lobster's pleopod system. Each pleopod pair has ample opportunity to maximize its own thrust production as a single unit, but can also exploit synergistic effects by interacting with its neighbours. The flow visualizations from the present study reinforce previous assertions that a metachronal system is more effective at creating propulsive currents than a single paddle (Barlow et al., 1993; Sleigh and Barlow, 1980). The unsteady motion of the pleopods produces a continuous, elongated jet wake. We report here that the magnitude of pleopod jet thrust is comparable to that generated by other proficient animal swimmers, and suggest, in accordance with other researchers's assertions, that the pleopods can produce forces large enough to contribute to locomotion. In the American lobster, the pleopods probably perform a secondary role in locomotion by contributing to a jet-assisted walking mechanism.

LIST OF ABBREVIATIONS

A_j	jet cross-sectional area
A_{pp}	pleopod projected area
a, b	Fourier series coefficients
C_d	coefficient of drag
D	force of drag
p	constant defining β as a function of time t in seconds
Re	Reynolds number
T	jet thrust
u_j	jet velocity
U_{pp}	pleopod speed relative to the fluid
$\beta(t)$	time-varying angle of the pleopod relative to the body's long axis
θ	angle of the protopod relative to the horizontal
ρ	fluid density

We thank the members of the StFX Biomechanics lab, especially R. Stanley for help with filming live lobsters, and J. Quinn, J. Williams, M. Chadwick, M. Ford, S. Mitchell and W. Quinn for helpful discussions on this work. We are grateful to W. Schnepf and C. Seaboyer for their technical expertise in constructing the lobster robot, and to A.-L. MacDonald and the StFX animal care staff for caring for our live lobsters. Also thanks to E. Tytell for providing us with his MatLab program. We also thank those who read and helped to improve later versions of the manuscript, including N. Danos, G. Lauder, and two anonymous reviewers. This project was funded by an NSERC of Canada Discovery grant to M.E.D. and an NSERC of Canada Master's PGS to J.L.L.

REFERENCES

Alexander, R. M. (1985). The maximum forces exerted by animals. *J. Exp. Biol.* **115**, 231-238.
Alexander, R. M. (2003). Modeling approaches in biomechanics. *Philos. Trans. R. Soc. Lond. B Biol. Sci.* **358**, 1429-1435.
Anderson, E. J. and DeMont, M. E. (2000). The mechanics of locomotion in the squid *Loligo pealei*: locomotory function and unsteady hydrodynamics of the jet and intramantle pressure. *J. Exp. Biol.* **203**, 2851-2863.
Anderson, E. J. and Grosenbaugh, M. A. (2005). Jet flow in steadily swimming adult squid. *J. Exp. Biol.* **208**, 1125-1146.
Atema, J. (1985). Chemoreception in the sea: adaptations of chemoreceptors and behaviour to aquatic stimulus conditions. *Symp. Soc. Exp. Biol.* **39**, 387-423.
Atema, J. and Voigt, R. (1995). Behaviour and sensory biology. In *Biology of the Lobster Homarus Americanus* (ed. J. R. Factor), pp. 313-348. San Diego, CA: Academic Press.
Ayers, J. (2004). Underwater walking. *Arthropod. Struct. Dev.* **33**, 347-360.
Barlow, D., Sleigh, M. A. and White, R. J. (1993). Water flows around the comb plates of the ctenophore *Pleurobranchia* plotted by computer: a model system for studying propulsion by antiplectic metachronism. *J. Exp. Biol.* **177**, 113-128.
Boudrias, M. A. (2002). Are pleopods just "more legs"? The functional morphology of swimming limbs in *Eurythenes gryllus* (Amphipoda). *J. Crustacean Biol.* **22**, 581-594.
Breithaupt, T. and Ayers, J. (1998). Visualization and quantification of biological flow fields through video-based digital motion-analysis techniques. *Mar. Freshw. Behav. Physiol.* **31**, 55-61.
Campbell, A. (1989). Dispersal of American lobsters, *Homarus americanus*, tagged off southern Nova Scotia. *Can. J. Fish. Aquat. Sci.* **46**, 1842-1844.
Cattaert, D. and Clarac, F. (1983). Influence of walking on swimmeret beating in the lobster *Homarus gammarus. J. Neurobiol.* **14**, 421-439.
Catton, K. B., Webster, D. R., Brown, J. and Yen, J. (2007). Quantitative analysis of tethered and free-swimming copepodid flow fields. *J. Exp. Biol.* **210**, 299-310.

Comeau, M. and Savoie, F. (2002). Movement of American lobster (*Homarus americanus*) in the southwestern Gulf of St. Lawrence. *Fish. Bull.* **100**, 181-192.

Cooper, R. A. and Uzmann, J. R. (1971). Migrations and growth of deep-sea lobsters, *Homarus americanus*. *Science* **171**, 288-290.

Copp, N. H. and Hodes, S. (2001). Asynchronous swimmeret beating during defense turns in the crayfish, *Procambarus clarkii*. *J. Comp. Physiol. A* **187**, 737-745.

Daniel, T. L. (1984). Unsteady aspects of aquatic locomotion. *Am. Zool.* **24**, 121-134.

Davis, W. J. (1968a). Lobster righting responses and their neural control. *Proc. R. Soc. Lond. B Biol. Sci.* **170**, 435-456.

Davis, W. J. (1968b). The neuromuscular basis of lobster swimmeret beating. *J. Exp. Zool.* **168**, 363-378.

Davis, W. J. (1968c). Quantitative analysis of swimmeret beating in the lobster. *J. Exp. Biol.* **48**, 643-662.

Davis, W. J. (1969). The neural control of swimmeret beating in the lobster. *J. Exp. Biol.* **50**, 99-117.

Dickinson, M. H. (1996). Unsteady mechanisms of force generation in aquatic and aerial locomotion. *Am. Zool.* **36**, 537-554.

Drucker, E. G. and Lauder, G. V. (1999). Locomotor forces on a swimming fish: three-dimensional vortex wake dynamics quantified using digital particle image velocimetry. *J. Exp. Biol.* **202**, 2393-2412.

Drucker, E. G. and Lauder, G. V. (2000). A hydrodynamic analysis of fish swimming speed: wake structure and locomotor force in slow and fast labriform swimmers. *J. Exp. Biol.* **203**, 2379-2393.

Ellenby, C. (1951). Body size in relation to oxygen consumption and pleopod beat in *Ligia oceanica* L. *J. Exp. Biol.* **28**, 492-507.

Frank, T. M. and Widder, E. A. (1994). Comparative study of behavioural sensitivity thresholds to near-UV and blue-green light in deep-sea crustaceans. *Mar. Biol.* **121**, 229-235.

Govind, C. K., Bevengut, M. and Pearce, J. (1995). Lobster swimmerets: muscle fiber composition and membrane definition of excitatory synapses in a predominantly fast system. *J. Exp. Zool.* **272**, 13-24.

Herrick, F. H. (1909). Natural history of the American lobster. *Bull. US Bur. Fish.* **29**, 149-408.

Johansson, L. C. and Lauder, G. V. (2004). Hydrodynamics of surface swimming in leopard frogs (*Rana pipiens*). *J. Exp. Biol.* **207**, 3945-3958.

Kils, U. (1981). Swimming behaviour, swimming performance and energy balance of Antarctic krill *Euphausia superba*. *BIOMASS Sci. Ser.* **3**, 1-122.

Koehl, M. A. R. (2003). Physical modeling in biomechanics. *Philos. Trans. R. Soc. Lond. B Biol. Sci.* **358**, 1589-1596.

Lim, J. L. (2006). *Jet-Assisted Walking in Lobsters.* Msc Thesis, Antigonish: St. Francis Xavier University, p. 97.

Lochhead, J. H. (1977). Unsolved problems of interest in the locomotion of Crustacea. In *Scale Effects in Animal Locomotion* (ed. T. J. Pedley), pp. 257-268. London: Academic Press.

MacCormack, T. J. and DeMont, M. E. (2003). Regional differences in allometric growth in Atlantic Canadian lobster (*Homarus americanus*). *J. Crustacean Biol.* **23**, 258-264.

Maude, S. H. and Williams, D. D. (1983). Behaviour of crayfish in water currents: hydrodynamics of eight species with reference to their distribution patterns in southern Ontario. *Can. J. Fish. Aquat. Sci.* **40**, 68-77.

McLaughlin, P. A. (1982). Comparative morphology of crustacean appendages. In *The Biology of Crustacea*, vol. 2 (ed. L. G. Abele), pp. 197-256. New York: Academic Press.

Mitchell, S. C. and DeMont, M. E. (2004). Modelling torque generation by the mero-carpopodite joint of the American lobster and the snow crab. *Mar. Freshw. Behav. Physiol.* **37**, 235-251.

Morris, M. J., Gust, G. and Torres, J. J. (1985). Propulsion efficiency and cost of transport for copepods: a hydromechanical model of crustacean swimming. *Mar. Biol.* **86**, 283-295.

Nauen, J. C. and Shadwick, R. E. (1999). The scaling of acceleratory aquatic locomotion: body size and tail-flip performance of the California spiny lobster *Panulirus interruptus*. *J. Exp. Biol.* **202**, 3181-3193.

Nauen, J. C. and Shadwick, R. E. (2001). The dynamics and scaling of force production during the tail-flip escape response of the California spiny lobster *Panulirus interruptus*. *J. Exp. Biol.* **204**, 1817-1830.

Nauwelaerts, S., Stamhuis, E. J. and Aerts, P. (2005). Propulsive force calculation in swimming frogs. I. A momentum-impulse approach. *J. Exp. Biol.* **208**, 1435-1443.

Press, W. H., Flannery, B. P., Teukolsky, S. A. and Vetterling, W. T. (1989). *Numerical Recipes in Pascal: The Art of Scientific Computing*. Cambridge: Cambridge University Press.

Sleigh, M. A. and Barlow, D. I. (1980). Metachronism and control of locomotion in animals with many propulsive structures. In *Aspects of Animal Movement* (ed. H. Y. Elder and E. R. Trueman), pp. 49-70. Cambridge: Cambridge University Press.

Stamhuis, E. J. and Nauwelaerts, S. (2005). Propulsive force calculations in swimming frogs II. Application of a vortex ring model to DPIV data. *J. Exp. Biol.* **208**, 1445-1451.

Stamhuis, E. J. and Videler, J. J. (1998a). Burrow ventilation in the tube-dwelling shrimp *Callianassa subterranea* (Decapoda: Thalassinidea). I. Morphology and motion of the pleopods, uropods and telson. *J. Exp. Biol.* **201**, 2151-2158.

Stamhuis, E. J. and Videler, J. J. (1998b). Burrow ventilation in the tube-dwelling shrimp *Callianassa subterranea* (Decapoda: Thalassinidea). II. The flow in the vicinity of the shrimp and the energetic advantages of a laminar non-pulsating ventilation current. *J. Exp. Biol.* **201**, 2159-2170.

Stamhuis, E. J. and Videler, J. J. (1998c). Burrow ventilation in the tube-dwelling shrimp *Callianassa subterranea* (Decapoda: Thalassinidea). III. Hydrodynamic modelling and the energetics of pleopod pumping. *J. Exp. Biol.* **201**, 2171-2181.

Talbot, P. and Helluy, S. (1995). Reproduction and embryonic development. In *Biology of the Lobster* (ed. J. R. Factor), pp. 177-216. San Diego, CA: Academic Press.

Thomasson, M. A., Johnson, M. L., Strömberg, J. O. and Gaten, E. (2003). Swimming capacity and pleopod beat rate as a function of sex, size and moult stage in Northern krill *Meganyctiphanes norvegica*. *Mar. Ecol. Prog. Ser.* **250**, 205-213.

van Duren, L. A. and Videler, J. J. (2003). Escape from viscosity: the kinematics and hydrodynamics of copepod foraging and escape swimming. *J. Exp. Biol.* **206**, 269-279.

Vogel, S. (1994). *Life in Moving Fluids: The Physical Biology of Flow*. Princeton, NJ: Princeton University Press.

Vogel, S. (2003). *Comparative Biomechanics: Life's Physical World*. Princeton, NJ: Princeton University Press.

Wootton, R. J. (1999). Invertebrate paraxial locomotory appendages: design, deformation and control. *J. Exp. Biol.* **202**, 3333-3345.

Yen, J. and Strickler, J. R. (1996). Advertisement and concealment in the plankton: what makes a copepod hydrodynamically conspicuous? *Invertebr. Biol.* **115**, 191-205.

Yen, J., Brown, J. and Webster, D. R. (2003). Analysis of the flow field of the krill, *Euphausia pacifica*. *Mar. Freshw. Behav. Physiol.* **36**, 307-319.